

Microscopic Mechanism and Pairing Symmetry of Superconductivity in the Noncentrosymmetric Heavy Fermion Systems CeRhSi₃ and CeIrSi₃

Yasuhiro TADA^{1*}, Norio KAWAKAMI^{1,2} and Satoshi FUJIMOTO²

¹*Department of Applied Physics, Osaka University, Suita, Osaka 565-0871, Japan*

²*Department of Physics, Kyoto University, Kyoto 606-8502, Japan*

We study the pairing symmetry of the noncentrosymmetric heavy fermion superconductors CeRhSi₃ and CeIrSi₃ under pressures, which are both antiferromagnets at ambient pressure. We solve the Eliashberg equation by means of the random phase approximation and find that the mixed state of extended *s*-wave and *p*-wave rather than the *d* + *f* wave state could be realized by enhanced antiferromagnetic spin fluctuations. It is elucidated that the gap function has line nodes on the Fermi surface and the resulting density of state in the superconducting state shows a similar character to that of usual *d*-wave superconductors, resulting in the NMR relaxation rate $1/(T_1T)$ that exhibits no coherence peak and behaves like $1/(T_1T) \propto T^2$ at low temperatures.

KEYWORDS: superconductivity, heavy fermion, without inversion symmetry

1. Introduction

Recent discoveries of heavy fermion superconductors without inversion symmetry have attracted much interest. CePt₃Si¹ was first identified and accompanied by the subsequent discoveries of CeRhSi₃,² CeIrSi₃,⁴ UIr⁵ and CeCoGe₃.⁶ Besides these heavy fermion systems, non-heavy fermion materials such as Li₂Pd₃B and Li₂Pt₃B were also found.⁷ In all these materials, there are nonzero potential gradient ∇V averaged in the unit cell due to lack of inversion symmetry, which results in the anisotropic spin-orbit interaction expressed as $e\hbar/4m^2c^2(\mathbf{k} \times \nabla V) \cdot \boldsymbol{\sigma}$ ($\equiv \alpha \mathcal{L}_0 \cdot \boldsymbol{\sigma}$), where \mathbf{k} is the momentum of a particle and $\boldsymbol{\sigma}$ is Pauli matrices. The anisotropic spin-orbit interaction $\mathcal{L}_0 \cdot \boldsymbol{\sigma}$, whose general form can be determined by a group theoretical argument,⁸ leads to many interesting phenomena.^{9–19} One of the outstanding properties is the parity mixing in superconducting states,^{9,11,13,14,18,19} *i.e.* the admixture of the spin-singlet and triplet states, which are both well defined in superconductors with inversion symmetry. The pairing symmetry in CePt₃Si has been studied both theoretically^{13,14,16,18,19} and experimentally^{20–24} and it is believed that the *s* + *p* wave superconducting state is realized. Frigeri *et al.*¹⁴ pointed out that the spin-orbit interaction could determine the direction of the *d*-vector as $\mathbf{d} \propto \mathcal{L}_0$ for which the highest transition temperature was obtained. A microscopic calculation with the detailed structure of the Fermi surface was done¹⁹ and it was concluded that *s* + *p* wave state is the most probable state.

Among this new kind of compounds, CeRhSi₃ and CeIrSi₃ have many similarities due to the same crystal structure: qualitatively similar pressure-temperature phase diagrams were indeed obtained from resistivity measurements.^{2,4} They are both in antiferromagnetic (AF) ordered states at low pressures, which are driven to the superconducting states beyond the critical pressures

where the Neel temperature rapidly decreases. The Neel temperature at ambient pressure is $T_N = 1.6\text{K}$ (5.0K) for CeRhSi₃ (CeIrSi₃) and the superconductivity appears in wide pressure ranges with approximate maximal transition temperature 1.1K at 2.6GPa (1.6K at 2.5GPa), respectively. Moreover, the NMR measurements of the relaxation rate $1/T_1$ for CeIrSi₃²⁸ suggest the existence of the AF spin fluctuations. Also, the neutron scattering experiments for CeRhSi₃²⁹ identified the AF ordering vectors as $\mathbf{Q} = (\pm 0.215, 0, 0.5)$ and it is concluded that the character of the AF is SDW-like. Besides these experiments, the recent band calculations elucidated that the above two compounds have very similar Fermi surfaces^{25,26}(FS). These similarities deduced both experimentally and theoretically motivate us to discuss the superconductivities of these two compounds in the same theoretical framework.

In this paper, we study the noncentrosymmetric superconductors CeRhSi₃ and CeIrSi₃ with particular emphasis on the influence of AF fluctuations to identify the pairing symmetry realized in these systems. We also examine the properties in the superconducting state, the density of states and the NMR relaxation rate which characterize the nodal structure of a gap function on the FS.

This paper is organized as follows. In the next section we introduce the model and briefly mention basic properties in the non-interacting case. Then in §3, we examine possible types of pairing symmetry by means of the random phase approximation. In §4, the characteristic properties in the superconducting state are discussed, and a brief summary is given in §5.

2. Model

In CeRhSi₃ and CeIrSi₃, heavy 4*f*-electrons around the Fermi level play important roles for low energy phenomena, where 4*f* electrons come from Ce ions forming a body-centered tetragonal(BCT) lattice² as shown in Fig. 1. For our analysis of the superconductivity, we start

*E-mail address: tada@tp.ap.eng.osaka-u.ac.jp

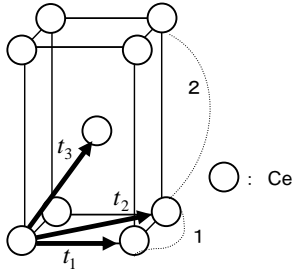


Fig. 1. Unit cell of CeRh(Ir)Si₃: only Ce sites (open circles) are shown for clarity, which form a body centered tetragonal lattice. t_1 , t_2 and t_3 are the nearest, the second nearest and the third nearest-neighbor hopping integrals, respectively. The ratio of the lattice constants is $a : b : c = 1 : 1 : 2$.

with the situation that heavy fermions have already been formed through hybridizations with conduction electrons and are described by an effective Hamiltonian. Although these materials have two kinds of the Fermi surfaces^{25–27} apart from the splitting by the spin-orbit interaction, we focus on one of them that has a large weight of the total density of states. This enables us to simply describe the electrons in the materials by the following single band model,

$$H = \sum_k \varepsilon_k c_k^\dagger c_k + U \sum_i n_{i\uparrow} n_{i\downarrow} + \alpha \sum_k c_k^\dagger \mathcal{L}_0(\mathbf{k}) \cdot \boldsymbol{\sigma} c_k, \quad (1)$$

$$\mathcal{L}_0(\mathbf{k}) = (\sin k_y, -\sin k_x, 0), \quad (2)$$

$$\varepsilon_k = -2t_1(\cos k_x + \cos k_y) + 4t_2 \cos k_x \cos k_y - 8t_3 \cos(k_x/2) \cos(k_y/2) \cos k_z - \mu, \quad (3)$$

where $c_k^{(\dagger)} = (c_{k\uparrow}, c_{k\downarrow})^{t(\dagger)}$ are the annihilation (creation) operators of the Kramers doublet. The third term of (2) is the Rashba-type anisotropic spin-orbit interaction due to the lack of inversion symmetry, where its coupling constant α is estimated to be less than $0.1\varepsilon_F$ (ε_F is the Fermi energy) according to the band calculation.²⁵ The bare Green's function in the normal state is

$$\hat{G}^0(k) = \sum_{\tau=\pm} \frac{\sigma_0 + (\mathcal{L}_0(\mathbf{k})/\|\mathcal{L}_0(\mathbf{k})\|) \cdot \boldsymbol{\sigma}}{2} G_\tau^0(k),$$

$$G_\tau^0(k) = \frac{1}{i\omega_n - \xi_{k\tau}},$$

$$\xi_{k\tau} = \varepsilon_k + \tau\alpha \|\mathcal{L}_0(\mathbf{k})\|,$$

$$\|\mathcal{L}_0(\mathbf{k})\| = \sqrt{\mathcal{L}_{0x}^2 + \mathcal{L}_{0y}^2 + \mathcal{L}_{0z}^2},$$

where $k = (i\omega_n, \mathbf{k})$. Note that the Green's functions have nonzero off-diagonal elements because of the spin-orbit interaction.

With a natural assumption deduced from the above-mentioned experimental and theoretical results that the AF in these materials are driven by the nesting of the Fermi surfaces, we choose the parameters in the above Hamiltonian t_1, t_2, t_3 and filling n so that our

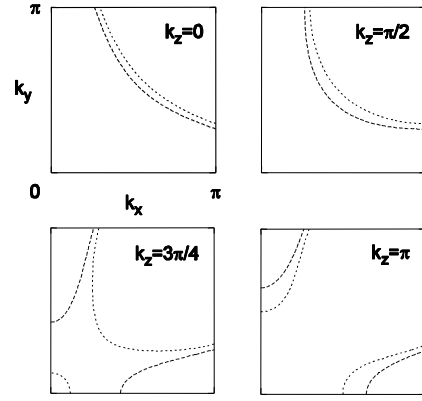


Fig. 2. Fermi surfaces in our model. The cross sections at $k_z = 0$, $k_z = \pi/2$, $k_z = 3\pi/4$ and $k_z = \pi$ are shown.

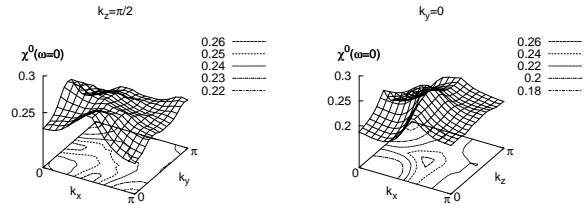


Fig. 3. Bare susceptibility $\chi^0(q)$ at $\omega = 0$ for $\alpha = 0$. The result is obtained for $T = 0.04$. The left (right) panel is $\chi^0(q)$ on the xy plane at $k_z = \pi/2$ (xz plane at $k_y = 0$)

model should be consistent with the band calculation and the neutron scattering experiment; $(t_1, t_2, t_3, n) = (1.0, 0.475, 0.3, 1.055)$. Here, we define t_1 as the energy unit. For these fixed parameters, the split Fermi surfaces with spin-orbit splitting $\sim 2\alpha$ are shown in Fig. 2. Our tight-binding model successfully reproduces the characteristic features of the Fermi surfaces obtained by the first principle band calculations.^{25–27} The matrix elements of the momentum-dependent susceptibility $\hat{\chi}^0(q)$ at $U = 0$ are expressed as,

$$\chi_{s_1 s_2 s_3 s_4}^0(q) = -\frac{T}{N} \sum_k G_{s_2 s_1}^0(q+k) G_{s_4 s_3}^0(k). \quad (4)$$

We show the bare susceptibility $\chi^0(q) \equiv \hat{\chi}_{\uparrow\uparrow\uparrow\uparrow}^0(q)$ for several choices of α at $\omega = 0$ in Figs. 3 and 4. At $\alpha = 0$, It has peaks around $\mathbf{Q}_{1\pm} \sim (\pm\pi/2, 0, \pi/2)$, $\mathbf{Q}_{2\pm} \sim (0, \pm\pi/2, \pi/2)$ as shown in Fig. 3. When the spin-orbit coupling α is turned on, the anisotropic spin-orbit splitting emerges, which suppresses the nesting of the FS and thus slightly affects the behavior of χ^0 : the peak structure is a little bit smeared, as seen from Fig. 4. The peak structure in $\hat{\chi}^0(q)$ is qualitatively in agreement with the neutron scattering experiment,²⁹ although its profile in momentum space is not so sharp in our model.

3. Pairing symmetry

In this section, we study the pairing symmetry by solving the Eliashberg equation which is expressed as

$$\lambda \Delta_{s_1 s_2}(k) = -\frac{T}{N} \sum_{k' s_3 s_4 \sigma_1 \sigma_2} V_{s_1 s_2 s_3 s_4}(k, k')$$

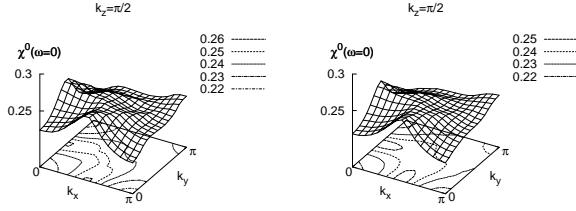


Fig. 4. Bare susceptibility $\chi^0(q)$ on the xy plane at $k_z = \pi/2$ and $\omega = 0$ for $\alpha \neq 0$ ($T = 0.04$). The left (right) panel is for $\alpha = 0.1$ (0.2).

$$\times G_{\sigma_1 s_3}^0(k') G_{\sigma_2 s_4}^0(-k') \Delta_{\sigma_1 \sigma_2}(k') (5)$$

where λ is the eigenvalue. We use the random phase approximation (RPA), which incorporates large AF fluctuations at the pressures near the AF critical point, to evaluate the effective pairing interaction V . In the following discussions, we neglect the normal self energy, which may have little influence on determining the pairing symmetry.³⁰ The effective pairing interaction V evaluated within RPA consists of three parts,

$$\begin{aligned} V_{s_1 s_2 s_3 s_4}(k, k') &= U \delta_{s_1 s_3} \delta_{s_2 s_4} \delta_{s_1 \bar{s}_2} \\ &+ V_{s_1 s_2 s_3 s_4}^{\text{bub}}(k, k') + V_{s_1 s_2 s_3 s_4}^{\text{lad}}(k, k'), \end{aligned} \quad (6)$$

where U is the bare Hubbard repulsion and V^{bub} , V^{lad} are calculated by collecting bubble and ladder diagrams, respectively. The bubble terms are

$$\begin{aligned} V_{ssss}^{\text{bub}}(k, k') &= v_{ssss}^{\text{bub}}(k - k') - v_{ssss}^{\text{bub}}(k + k'), \\ V_{s\bar{s}s\bar{s}}^{\text{bub}}(k, k') &= v_{s\bar{s}s\bar{s}}^{\text{bub}}(k - k'), \end{aligned}$$

where

$$\begin{aligned} v_{ssss}^{\text{bub}}(q) &= -U^2 \chi_{s\bar{s}s\bar{s}}^0(q) / D_{\text{bub}}(q), \\ v_{s\bar{s}s\bar{s}}^{\text{bub}}(q) &= U^2 (-\chi_{s\bar{s}s\bar{s}}^0(q) - U \chi_{s\bar{s}s\bar{s}}^0(q) \chi_{s\bar{s}s\bar{s}}^0(q)) \\ &+ U \chi_{s\bar{s}s\bar{s}}^0(q) \chi_{ssss}^0(q) / D_{\text{bub}}(q), \\ D_{\text{bub}}(q) &= (1 + U \chi_{\uparrow\uparrow\downarrow\downarrow}^0(q)) (1 + U \chi_{\downarrow\downarrow\uparrow\uparrow}^0(q)) \\ &- U^2 \chi_{\uparrow\uparrow\uparrow\uparrow}^0(q) \chi_{\downarrow\downarrow\downarrow\downarrow}^0(q) \end{aligned}$$

and $V_{s_1 s_2 s_3 s_4}^{\text{bub}}$ with other spin indices are zero. The ladder terms are

$$\begin{aligned} V_{s\bar{s}s\bar{s}}^{\text{lad}}(k, k') &= v_{s\bar{s}s\bar{s}}^{\text{lad}}(k - k') - v_{s\bar{s}s\bar{s}}^{\text{lad}}(k + k'), \\ V_{s\bar{s}s\bar{s}}^{\text{lad}}(k, k') &= v_{s\bar{s}s\bar{s}}^{\text{lad}}(k - k'), \end{aligned}$$

where

$$\begin{aligned} v_{s\bar{s}s\bar{s}}^{\text{lad}}(q) &= U^2 \chi_{s\bar{s}s\bar{s}}^0(q) / D_{\text{lad}}(q), \\ v_{s\bar{s}s\bar{s}}^{\text{lad}}(q) &= U^2 (\chi_{s\bar{s}s\bar{s}}^0(q) - U \chi_{s\bar{s}s\bar{s}}^0(q) \chi_{s\bar{s}s\bar{s}}^0(q)) \\ &+ U \chi_{s\bar{s}s\bar{s}}^0(q) \chi_{ssss}^0(q) / D_{\text{lad}}(q), \\ D_{\text{lad}}(q) &= (1 - U \chi_{\downarrow\downarrow\uparrow\uparrow}^0(q)) (1 - U \chi_{\uparrow\uparrow\downarrow\downarrow}^0(q)) \\ &- U^2 \chi_{\uparrow\uparrow\downarrow\downarrow}^0(q) \chi_{\downarrow\downarrow\uparrow\uparrow}^0(q) \end{aligned}$$

and others are zero. Within RPA, only the $V_{s\bar{s}s\bar{s}}^{\text{lad}}$ terms do not conserve the spins of two particles before and after scattering, and the parity mixing is driven only by two

Green's functions which connect the 4-point vertex part with the gap function in eq.(5). Thus, the parity mixing effect may not be strongly enhanced by U .

Generally, the gap function $\Delta_{s_1 s_2}(k)$ is expressed as,

$$\Delta(k) = (\Delta_s(i\omega_n) d_0(\mathbf{k}) \sigma_0 + \Delta_t(i\omega_n) \mathbf{d}(\mathbf{k}) \cdot \boldsymbol{\sigma}) i\sigma_2, \quad (7)$$

where $\Delta_s d_0$ and $\Delta_t \mathbf{d}$ are the order parameters for singlet and triplet states, which can have non-zero values simultaneously because of the Rashba spin-orbit interaction. We denote $(d_\mu)_{\mu=0\sim 3} = (d_0, \mathbf{d})$ hereafter. We can determine, by solving the above eigenvalue equation (5), the symmetry of the gap function and the transition temperature T_c at which the maximum eigenvalue λ_{max} reaches unity.

The pairing symmetries of the singlet states $\{d_0^\Gamma(\mathbf{k})\}_\Gamma$ for five irreducible representations of C_{4v} are listed in Table I. Here, we choose $\{\mathbf{d}^\Gamma(\mathbf{k})\}_\Gamma$ as $\mathbf{d}^\Gamma(\mathbf{k}) = d_0^\Gamma(\mathbf{k}) \mathcal{L}_0(\mathbf{k})$

Irreducible representation	Basis function
A_1 (extended s)	$d_0^{A_1}(\mathbf{k}) = \cos 2k_z$
A_2 ($g_{xy}(x^2 - y^2)$)	$d_0^{A_2}(\mathbf{k}) = \sin 2k_x \sin 2k_y (\cos 2k_x - \cos 2k_y)$
B_1 ($d_{x^2 - y^2}$)	$d_0^{B_1}(\mathbf{k}) = (\cos 2k_x - \cos 2k_y)$
B_2 (dx_y)	$d_0^{B_2}(\mathbf{k}) = \sin 2k_x \sin 2k_y$
E (dx_z)	$d_0^E(\mathbf{k}) = \sin k_x \sin 2k_z$
every representation	$\mathbf{d}^\Gamma(\mathbf{k}) = d_0^\Gamma(\mathbf{k}) \mathcal{L}_0(\mathbf{k})$

Table I. The irreducible representations of C_{4v} and the basis functions.

for each representation which is considered to be most stable in the superconductors with $\Delta \ll \alpha$.^{14,16} The harmonic wave functions in Table I give the largest contributions among the functions which belong to a given symmetry, mainly because of the factor 1/2 in the propagating vectors $\mathbf{Q}_{1,2\pm}$.

We solve the Eliashberg equation for all symmetries and trace each maximum eigenvalue $\{\lambda^\Gamma\}_\Gamma$ with increasing U at fixed temperature $T = 0.04$. In the calculation, the first Brillouin zone is divided into $16 \times 16 \times 16$ meshes and the number of the Matsubara frequencies used is 512. We have checked that the following results are qualitatively unchanged for 512 Matsubara frequencies and $(32)^3$ \mathbf{k} -meshes. In Fig. 5, $\lambda(U, T = 0.04)$ at $\alpha = 0$ are shown for five irreducible representations. In the case of $\alpha = 0$, the Eliashberg equation (5) is separated into singlet and triplet parts and solved independently. For singlet superconductivity, we can see that, among five symmetries, only $\lambda_{\text{sin}}^{A_1}$ for $d_0^{A_1} = \cos 2k_z$ (extended s -wave) can reach unity. Other λ_{sin} are much smaller than $\lambda_{\text{sin}}^{A_1}$, and we cannot see any significant difference among them in the present calculation. Regarding the triplet part, all λ_{tri} are small and none of them can reach unity.

We remark that, for A_1 representation, $\lambda_{\text{tri}}^{A_1}$ for $\mathbf{d}^{A_1}(\mathbf{k}) = d_0^{A_1}(\mathbf{k}) \mathcal{L}_0(\mathbf{k})$ is very small and negative, which means that the triplet (p -wave) channel in the effective interaction V is weakly repulsive.

Let us now inspect the effect of anisotropic spin-orbit interaction for A_1 symmetry, by computing $\lambda(U, T =$

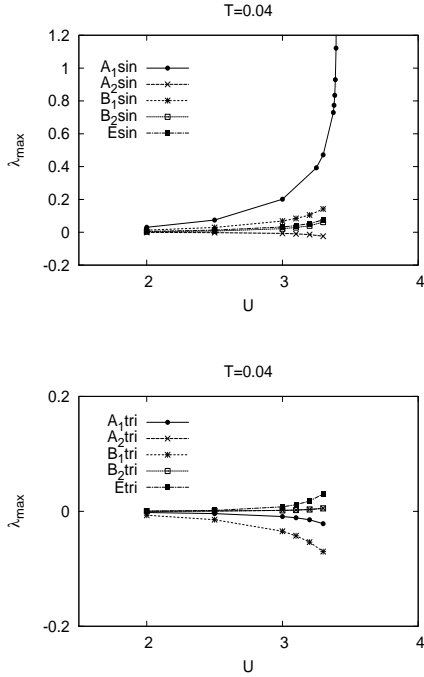


Fig. 5. Maximum eigenvalues of the Eliashberg equation for five irreducible representations as a function of U with $\alpha = 0$ and $T = 0.04$. The upper (lower) panel is λ_{\max}^{Γ} for the singlet (triplet) gap function.

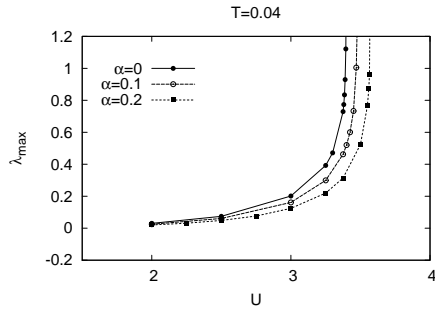


Fig. 6. Maximum eigenvalues λ^{A_1} for $\alpha = 0, 0.1, 0.2$ at $T = 0.04$. For $\alpha = 0$, λ is shown only for the singlet gap function, while for $\alpha \neq 0$, λ is for the singlet-triplet mixing state.

0.04) at $\alpha = 0, 0.1, 0.2$. The results are shown in Fig. 6. Critical values of U , which correspond to the critical pressure for the AF transition, increase a little with α , reflecting the change of FS that has a tendency to suppress $\hat{\chi}^0$. Note that, within RPA calculations, the effective Coulomb interaction $U_{\text{eff}} = U/\min(1 - U\hat{\chi}^0(Q))$ is a relevant parameter controlling spin fluctuations even in the presence of α . We see that λ^{A_1} decreases with increasing α mainly due to the suppressed U_{eff} at the same value of U and also due to the mixing with the repulsive triplet channel. However, it remains larger than unity, suggesting the possibility of the A_1 -symmetric superconductivity. The ratio of the amplitudes of the singlet gap function and the triplet gap function for A_1 symmetry is very small $\Delta_t/\Delta_s \lesssim 0.01$ for $\alpha \neq 0$, which means that the properties of the superconductivity is characterized

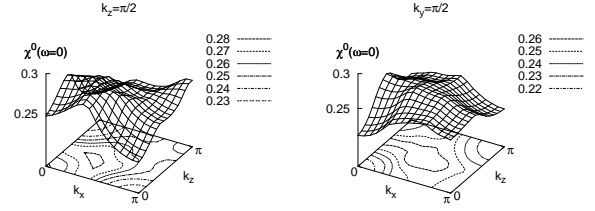


Fig. 7. Bare susceptibility $\chi^0(q) \equiv \chi_{\uparrow\uparrow\uparrow\uparrow}^0(q)$ at $\omega = 0$ and $T = 0.04$ with $(t_1, t_2, t_3, n, \alpha) = (1.0, 0.405, 0.3, 1.057, 0.1)$. The left (right) panel is $\chi^0(q)$ on the xy plane at $k_z = \pi/2$ (the xz plane at $k_y = \pi/2$).

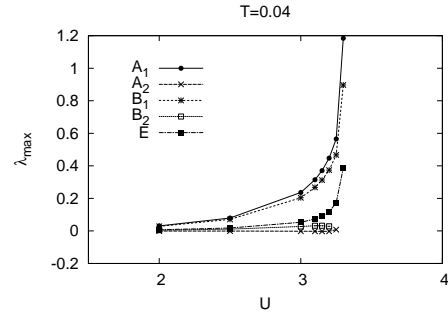


Fig. 8. Maximum eigenvalues λ for five irreducible representations with $(t_1, t_2, t_3, n, \alpha) = (1.0, 0.405, 0.3, 1.057, 0.1)$ at $T = 0.04$.

dominantly by the singlet part.

Generally, the A_1 symmetric gap function has line nodes perpendicular to c -axis on the Fermi surface, but the averaged value over the FS $\langle d_{\mu}^{A_1} \rangle_{\text{FS}}$ has a non-zero value. In our model with this gap function, there exist line nodes at $k_z = \pm\pi/4, \pm 3\pi/4$ on the FS. Regarding the nodal structure, our A_1 gap function $d_{\mu}^{A_1}$ is very similar to that for the usual d -wave superconductivity.

Because the neutron scattering experiment²⁹ was performed at ambient pressure, and the true propagating vector under pressures is unknown while the superconductivity occurs at high pressures, we also examine the pairing symmetry with another set of parameters $(t_1, t_2, t_3, n) = (1.0, 0.405, 0.3, 1.057)$ which give maximum values of $\chi^0(q)$ at $\mathbf{Q}' \sim (0.35\pi, 0.35\pi, 0.5\pi)$ as shown in Fig. 7. This ordering vector lifts the degeneracy of $\mathbf{Q}_1 \sim (0.5\pi, 0, 0.5\pi)$ and $\mathbf{Q}_2 \sim (0, 0.5\pi, 0.5\pi)$ in the xy components. We show λ calculated for five irreducible representations at $\alpha = 0.1$ in Fig. 8. In this case, we again find that the A_1 -symmetric pairing state is most likely to appear, which asserts the robustness of the stability of the pairing state with the A_1 symmetry against a slight change of the Fermi surface. B_1 symmetry is the second probable candidate because the gap function $d_0^{B_1} = \cos(2k_x) - \cos(2k_y)$ is favorable with the propagating vector $\mathbf{Q}'_x = \mathbf{Q}'_y \sim 0.35\pi$ which could lead to the sign change $d_0^{B_1}(\mathbf{k}) \cdot d_0^{B_1}(\mathbf{k} + \mathbf{Q}') < 0$ on some regions $\{\mathbf{k} \in \text{FS}\}$. We calculate $\{\lambda^{\Gamma}\}$ for other sets of parameters with which the propagating vector is of the form $\mathbf{Q} = (\delta, \delta, \pi/2)$ or $(\delta, 0, \pi/2)$ and confirmed that A_1 -symmetric superconductivity is the most probable.

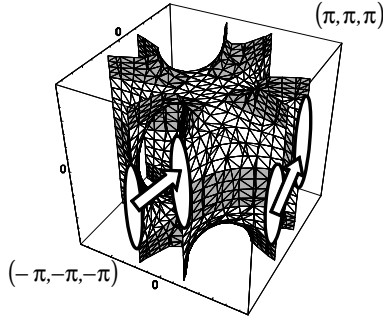


Fig. 9. Fermi surface for $(t_1, t_2, t_3, n, \alpha) = (1.0, 0.475, 0.3, 1.05, 0)$. The gray regions and white regions correspond to $d_0^{A_1} = \cos 2k_z > 0$, $d_0^{A_1} < 0$ respectively. The line nodes of the A_1 gap function are located on the boundaries between the two regions. The white arrows connecting the areas enclosed by contours represent the scattering processes associated with the propagating vector $\mathbf{Q}_{1,2\pm}$.

This is because $d_0^{A_1} = \cos 2k_z$ depends only on k_z and the changes in the x, y components of \mathbf{Q} do not affect the main scattering processes for the A_1 -symmetric superconductivity. Thus, unless the effects of pressures are not restricted to the fluctuations in the xy components of \mathbf{Q} , it is most stable.

Let us consider a possible explanation for the stability of the superconductivity with this symmetry in the case of $(t_1, t_2, t_3, n, \alpha) = (1.0, 0.475, 0.3, 1.05, 0)$. We think that, in our model, taking into account only the scattering processes with $\mathbf{k} \pm \mathbf{k}' = \mathbf{Q}_{1,2\pm}$ gives us intuitive but restricted information, because the peak structures of $\hat{\chi}_0(q)$ are not so sharp and the shape of the FS is complicated in the 3D momentum space. Nevertheless we try to figure out how these scattering processes on the FS contribute to the realization of the superconductivity with the A_1 symmetry. Figure 9 shows the FS and the signs of the singlet A_1 gap function $d_0^{A_1} = \cos 2k_z$; the gray and the white regions correspond to $d_0^{A_1} = \cos 2k_z > 0$ and $d_0^{A_1} < 0$, respectively. The FS has a cylinder-like shape along z -axis and there exist wide ranges of hot spots. Among these regions, the subsets of the FS connected to each other via the momentum \mathbf{Q} play an important role for the superconductivity, when $d_0^{A_1}(\mathbf{k}) \cdot d_0^{A_1}(\mathbf{k} \pm \mathbf{Q})$ is negative and large. Such spots might be on the sides of the cylinder-like FS as shown in Fig. 9 (enclosed by contours) and the area of the spots could be large. Thus, the scattering processes drawn with white arrows in Fig. 9 could mediate the superconductivity.

4. Density of states and NMR relaxation rate

We now turn to the properties in the superconducting state: the density of states $\rho(\omega)$ and the NMR relaxation rate $1/T_1T$ with A_1 symmetry $d_\mu^{A_1}$. They are expressed as,¹⁶

$$\rho(\omega) = \frac{1}{\pi} N_n(\omega), \quad (8)$$

$$\frac{1}{T_1T} \propto \int \frac{d\omega}{2\pi} \frac{1}{2T \cosh^2 \frac{\omega}{2T}} \left(|N_n(\omega)|^2 + |N_a(\omega)|^2 \right) \quad (9)$$

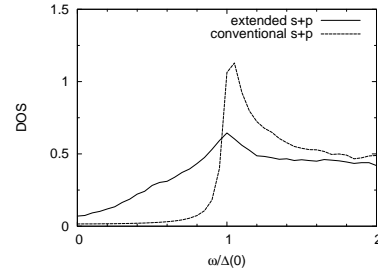


Fig. 10. The density of states in the superconducting state with $\Delta_s(0) = 2.0T_c$, $\Delta_t(0)/\Delta_s(0) = 0.01$ and $\gamma = 0.01\Delta_s(0)$. The solid line is for the A_1 -symmetric superconducting state and the dashed line is for the conventional $s + p$ wave state.

where

$$N_n(\omega) = - \sum_{k\tau} \text{Im} G_\tau^{0R}(\omega + i\gamma, \mathbf{k}),$$

$$N_a(\omega) = - \sum_{k\tau} \text{Im} F_\tau^{0R}(\omega + i\gamma, \mathbf{k}).$$

The normal and anomalous Green's functions in the superconducting state are given by

$$G_\tau^0(k) = \frac{i\omega_n + \xi_{k\tau}}{(i\omega_n)^2 - E_{k\tau}^2},$$

$$F_\tau^0(k) = \frac{\Delta_{k\tau}}{(i\omega_n)^2 - E_{k\tau}^2},$$

with

$$E_{k\tau} = \sqrt{\xi_{k\tau}^2 + \Delta_{k\tau}^2},$$

$$\Delta_{k\tau} = \Delta_s(T) d_0(\mathbf{k}) + \tau \Delta_t(T) \|\mathbf{d}(\mathbf{k})\|.$$

We assume the T dependence of the order parameters as $\Delta_\mu(T) = \Delta_\mu(0) \tanh\left(1.74\sqrt{T_c/T - 1}\right)$, regarding $\Delta_\mu(0)$ and the quasiparticle damping factor γ as fitting parameters. In Fig. 10, the density of states for the extended $s + p$ wave superconducting state is shown, which is compared with that of the conventional $s + p$ wave state. In contrast to the conventional $s + p$ -wave state, the peak of $\rho(\omega)$ at $\omega \sim \Delta$ is largely suppressed and the behavior at $\omega \sim 0$ is proportional to ω in our system. The latter aspect directly follows from the existence of line nodes for the A_1 -symmetric gap function. As for the former effect, one notices that the strong suppression of $\rho(\omega)$ makes its profile quite similar to that in usual d -wave states. This means that, in CeRhSi₃ and CeIrSi₃, bulk properties which reflect the nodal structure of the gap function may show no essential difference from those for d -wave superconductors.

Next, we proceed to discuss the NMR relaxation rate $1/(T_1T)$. Since $1/(T_1T)$ generally depends on $N_n(\omega)$ and $N_a(\omega)$ not only at $\omega \sim 0$ but also at $\omega \sim \Delta(0)$, the existence of line nodes does not necessarily mean that $1/T_1T$ in the extended $s + p$ wave superconducting state is similar to that in d -wave states. Figure 11 shows the temperature dependence of $1/(T_1T)$ normalized by $1/(T_1T)_c$

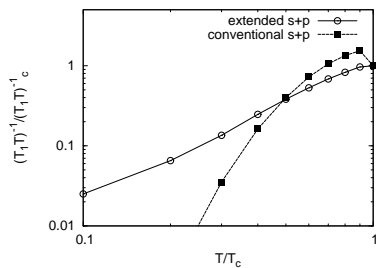


Fig. 11. NMR relaxation rate $1/T_1T$ as a function of T . The amplitude of the gap function at $T = 0$ and the quasiparticle damping factor are chosen as $\Delta_s(0) = 2.0T_c$, $\Delta_t(0)/\Delta_s(0) = 0.01$ and $\gamma = 0.01\Delta_s(0)$. The line with open circles is for the A_1 -symmetric superconducting state and the line with black squares is for the conventional $s + p$ wave state.

for the A_1 -symmetric superconducting state and the conventional $s + p$ wave state. By repeating similar calculations for several choices of $(\Delta(0), \gamma)$, we find that $1/T_1T$ with A_1 -symmetric gap function has no coherence peak and behaves as $1/(T_1T) \sim T^2$, which is characteristic of line-node superconductors. This behavior of the NMR $1/(T_1T)$ is usually typical for dominant d -wave superconductivity but not for dominant extended s -wave one. In the present system, however, the FS is highly anisotropic and the A_1 gap function with line nodes could effectively behave like a d -wave gap function on the FS.

According to the recent NMR experiments for CeIrSi_3 ,²⁸ $1/(T_1T)$ exhibits line-node behavior with no coherence peak, which seems not contradictory to our results.

5. Summary

We have studied the pairing symmetry and the nature of the gap function in the superconducting state in the nonsymmorphic heavy fermion superconductors CeRhSi_3 and CeIrSi_3 . Solving the Eliashberg equation within RPA, we have found that AF fluctuations could mediate the superconductivity with the parity mixing of the extended s -wave and p -wave states rather than the $d + f$ wave state through the Rashba spin-orbit interaction. We have confirmed that extended $s + p$ wave state is robust against a slight change of the Fermi surface under pressure. In the superconducting state, the density of states $\rho(\omega)$ is very similar to that in d -wave superconducting states; suppressed $\rho(\omega \sim \Delta)$ and $\rho(\omega \sim 0) \propto \omega$. Furthermore, the NMR relaxation rate exhibits $1/(T_1T) \propto T^2$ with no coherence peak at T_c as in the case of the usual d -wave superconductivity. Our results suggest a possible understanding of the recent NMR experiment within the extended $s + p$ wave state.

In the present paper, the effects of the normal self-energy are not taken into account. According to the recent experimental observations, the strong-coupling effect may be important in CeRhSi_3 and CeIrSi_3 .^{31,32} We would like to address this issue in the near future.

Acknowledgement

We thank M. Sigrist, N. Kimura, H. Mukuda, H. Harima, T. Terashima, H. Yamagami, and Y. Onuki for

valuable discussions. Numerical calculations were partially carried out at the Yukawa Institute Computer Facility.

- 1) E. Bauer, G. Hilscher, H. Michor, Ch. Paul, E. W. Scheidt, A. Griбанov, Yu. Seropegin, H. Noël, M. Sigrist, and P. Rogl: Phys. Rev. Lett. **92** (2004) 3129.
- 2) N. Kimura, K. Ito, K. Saitoh, Y. Umeda, H. Aoki, and T. Terashima: Phys. Rev. Lett. **95** (2005) 247004.
- 3) Y. Muro, M. Ishikawa, K. Hirota, Z. Hiroi, N. Takeda, N. Kimura, and H. Aoki: J. Phys. Soc. Jpn. **76** (2007) 033706.
- 4) I. Sugitani, Y. Okuda, H. Shishido, T. Yamada, A. Thamizhavel, E. Yamamoto, T. D. Matsuda, Y. Haga, T. Takeuchi, R. Settai, and Y. Ōnuki: J. Phys. Soc. Jpn. **75** (2006) 043703.
- 5) T. Akazawa, H. Hidaka, H. Kotegawa, T. Kobayashi, T. Fujiwara, E. Yamamoto, Y. Haga, R. Settai, and Y. Ōnuki: J. Phys. Soc. Jpn. **73** (2004) 3129.
- 6) R. Settai, I. Sugitani, Y. Okuda, A. Thamizhavel, M. Nakashima, Y. Ōnuki, and H. Harima: J. Mag. Mag. Matt. **310** (2007) 844.
- 7) K. Togano, P. Badica, Y. Nakamori, S. Orimo, H. Takeya, and K. Hirata: Phys. Rev. Lett. **93** (2004) 247004.
- 8) K. Samokhin: Phys. Rev. Lett. **94** (2005) 024515.
- 9) V. M. Edelstein: Sov. Phys. JETP. **68** (1989) 1244.
- 10) V. M. Edelstein: Phys. Rev. Lett. **75** (1995) 2004.
- 11) L. P. Gor'kov and E. Rashba: Phys. Rev. Lett. **87** (2001) 037004.
- 12) S. K. Yip: Phys. Rev. B **65** (2002) 144508.
- 13) M. Sigrist, D. F. Agterberg, P. A. Frigeri, N. Hayashi, R. P. Kaur, A. Koga, I. Milat, and K. Wakabayashi: AIP Conference Proceedings **816** (2006) 124.
- 14) P. A. Frigeri, D. F. Agterberg, A. Koga, and M. Sigrist: Phys. Rev. Lett. **92** (2004) 097001.
- 15) R. P. Kaur, D. F. Agterberg, and M. Sigrist: Phys. Rev. Lett. **94** (2005) 137002.
- 16) S. Fujimoto: Phys. Rev. B. **72** (2005) 024515.
- 17) S. Fujimoto: J. Phys. Soc. Jpn. **75** (2006) 083704.
- 18) S. Fujimoto: J. Phys. Soc. Jpn. **76** (2007) 051008.
- 19) Y. Yanase *et al.*: J. Phys. Soc. Jpn. **76** (2007) 043712.
- 20) M. Yogi, Y. Kitaoka, S. Hashimoto, T. Yasuhida, R. Settai, T. D. Matsuda, Y. Haga, Y. Ōnuki, P. Rogl, and E. Bauer: Phys. Rev. Lett. **93** (2004) 027003.
- 21) M. Yogi, H. Mukuda, Y. Kitaoka, S. Hashimoto, T. Yasuhida, R. Settai, T. D. Matsuda, Y. Haga, Y. Ōnuki, P. Rogl, and E. Bauer: J. Phys. Soc. Jpn. **75** (2006) 013709.
- 22) K. Izawa, Y. Kasahara, Y. Matsuda, K. Behnia, T. Yasuhida, R. Settai, and Y. Ōnuki: Phys. Rev. Lett. **94** (2005) 197002.
- 23) T. Takeuchi, M. Tsujino, T. Yasuda, S. Hashimoto, R. Settai, and Y. Ōnuki: J. Mag. Mag. Matt. **310** (2007) 557.
- 24) I. Bonalde, W. Brämer-Escamilla, and E. Bauer: Phys. Rev. Lett. **94** (2005) 207002.
- 25) H. Harima: *private communication*.
- 26) T. Terashima, Y. Takahide, T. Matsumoto, and S. Uji: to be published in Phys. Rev. B
- 27) H. Yamagami: *private communication*.
- 28) H. Mukuda, T. Fujii, A. Harada, T. Ohara, M. Yashima, Y. Kitaoka, Y. Okuda, R. Settai, and Y. Ōnuki: *unpublished*.
- 29) N. Aso, H. Miyano, H. Yoshizawa, N. Kimura, T. Komatsubara, and H. Aoki: J. Mag. Mag. Matt. **310** (2007) 602.
- 30) Y. Yanase, T. Jujo, T. Nomura, H. Ikeda, T. Hotta, K. Yamada: Phys. Rep. **387** (2004) 1.
- 31) N. Kimura, K. Ito, H. Aoki, S. Uji, and T. Terashima: Phys. Rev. Lett. **98** (2007) 197001.
- 32) N. Tateiwa, Y. Haga, T. D. Matsuda, S. Ikeda, E. Yamamoto, Y. Okuda, Y. Miyauchi, R. Settai, and Y. Onuki: J. Phys. Soc. Jpn. **76** (2007) 083706.